DISCLAIMER

This draft chapter is a work in progress and is being provided to the public for information purposes only. Because it is a work in progress, there are parts that are either missing or will be revised, and the page numbers will change. Permission to cite any part of this work must be obtained from the prime author. The final version of this chapter will be published in Volume 9 of the *SeaWiFS Postlaunch Technical Report Series*.

Chapter 8

The SeaWiFS Atmospheric Correction Algorithm Updates

Menghua Wang
University of Maryland, Baltimore County, Baltimore, Maryland

Abstract

Some updates of the SeaWiFS atmospheric correction for the reprocessing are described in this chapter, in particular, the updates of the aerosol lookup tables, the atmospheric diffuse transmittance tables, the ocean whitecap computations, and the implementation of new Rayleigh radiance tables which were generated including the various ocean surface wind speeds. In addition, computation of a new SeaWiFS atmospheric product, the Ångström exponent, is described. These modifications significantly improve the SeaWiFS retrieval results.

8.1 INTRODUCTION

It is well known that atmospheric correction, which removes more than 90% of sensor-measured signals contributed from the atmosphere in the visible spectrum, is the key procedure in ocean color imagery data processing. With the successful launch of the SeaWiFS (Hooker et al. 1992 and McClain et al. 1998) on 1 August 1997 and its data processing since then, it is very important to reevaluate and update the SeaWiFS atmospheric corrections. The SeaWiFS atmospheric correction algorithm uses two near-infrared (NIR) bands (765 and 865 nm) to estimate the aerosol optical properties and extrapolate these into the visible spectrum (Gordon and Wang 1994b). The implementation of the algorithm was achieved by using lookup tables for Rayleigh scattering, aerosol contributions, and the effects of the atmospheric diffuse transmittance. The ocean whitecap contributions at the SeaWiFS bands were estimated using the reflectance model. In this chapter, a brief overview of the SeaWiFS atmospheric correction algorithm is given. Then, outlines are given of some updates and modifications in the aerosol lookup tables, the atmospheric diffuse transmittance tables, and computations of the whitecap contributions.

8.2 ALGORITHM

To better describe the SeaWiFS atmospheric correction algorithm and its implementation into the data processing system, the reflectance $\rho = \pi L / \cos\theta_0 F_0$ is defined, where L is the radiance in a given solar and viewing geometry, F_0 is the extraterrestrial solar irradiance, and θ_0 is the solar zenith angle. The SeaWiFS measured reflectance at the top of the ocean–atmosphere system can be written as:

$$\begin{aligned}\rho_t(\lambda) \;&= \rho_r(\lambda) \;+\; \rho_a(\lambda) \;+\; \rho_{ra}(\lambda) \\ &\quad +\; t(\lambda)\rho_{wc}(\lambda) \;+\; t(\lambda)\rho_w(\lambda)\end{aligned}, \qquad (1)$$

where $\rho_r(\lambda)$, $\rho_a(\lambda)$, and $\rho_{ra}(\lambda)$ are the contributions from multiple scattering of air molecules (Rayleigh scattering), aerosols, and Rayleigh-aerosol interactions, respectively. The $\rho_{wc}(\lambda)$ is the reflectance at the sea surface which arises from sunlight and skylight reflecting from whitecaps on the surface (Gordon and Wang 1994a) and $\rho_w(\lambda)$ is the water-leaving reflectance, which is the desired quantity in ocean color remote sensing. The $t(\lambda)$ is the atmospheric diffuse transmittance (Wang 1999, and Yang and Gordon 1997) which accounts for the effects of propagating water-leaving and whitecap reflectances from the sea surface to the top of the atmosphere (TOA). In (1), the surface sun glint term has been ignored.

Because more than 90% of the signal in the visible spectrum measured at satellite altitude, is contributed by the atmosphere and ocean surface effects—the first four terms in (1)—accurately removing these effects is crucial to the success of any ocean color remote sensing experiment. The SeaWiFS atmospheric correction algorithm (Gordon and Wang 1994b) uses the two SeaWiFS NIR bands centered at 765 and 865 nm to estimate the atmospheric effects and extrapolate these into the visible spectrum. Unlike Rayleigh scattering, which can be computed accurately, aerosol scattering is highly variable, and the effects of $\rho_a(\lambda) \;+\; \rho_{ra}(\lambda)$ in (1) on the imagery cannot be predicted a priori. The water-leaving reflectance $\rho_w(\lambda)$ at the two NIR bands, however, is usually negligible because of strong water absorption. The radiances measured at these two NIR bands, therefore, are essentially the contributions from the atmosphere. For the SeaWiFS, two NIR channels, (1) can be written as

$$\rho_t(\lambda) - \rho_r(\lambda) - t(\lambda)\rho_{wc}(\lambda) = \rho_a(\lambda) + \rho_{ra}(\lambda). \qquad (2)$$

The effects of aerosols and Rayleigh-aerosol interactions, $\rho_a(\lambda) + \rho_{ra}(\lambda)$, in the imagery, therefore, can be estimated

at the two NIR bands from the sensor-measured radiances, the computed Rayleigh scattering reflectances, and the estimated whitecap contributions (Gordon and Wang 1994a). This quantity is then extrapolated and removed in the visible. The extrapolation was achieved through a process of aerosol model selection from evaluating the atmospheric correction parameters, $\epsilon(\lambda_i, \lambda_j)$, defined as (Gordon and Wang 1994b, and Wang and Gordon 1994)

$$\epsilon(\lambda_i, \lambda_j) \;=\; \frac{\rho_{as}(\lambda_i)}{\rho_{as}(\lambda_j)}, \tag{3}$$

where $\rho_{as}(\lambda_i)$ and $\rho_{as}(\lambda_j)$ are the single scattering aerosol reflectances at wavelengths λ_i and λ_j, respectively. The λ_j is usually taken at the longer NIR band, i.e., 865 nm for SeaWiFS. The value of $\epsilon(\lambda_i, \lambda_j)$ characterizes the spectral variation of aerosol extinction coefficient which include the aerosol optical thickness, single scattering albedo, and the aerosol scattering phase function. It, therefore, forms the link between the value of $\epsilon(\lambda_i, \lambda_j)$ and the aerosol model.

The implementation of the Gordon and Wang algorithm into the SeaWiFS data processing system was achieved through the use of lookup tables based on a large number (≈25,000) of radiative transfer simulations which use the aerosol models developed by Shettle and Fenn (1979). The main lookup tables contain information on the $\rho_a(\lambda) + \rho_{ra}(\lambda)$ values for various aerosol optical and microphysical properties (number of different aerosol models with various aerosol optical thicknesses) and solar and viewing geometries at the eight SeaWiFS spectral bands. There are two other tables which are much smaller in size are the Rayleigh radiance tables, $\rho_r(\lambda)$, and the atmospheric diffuse transmittance tables, $t(\lambda)$.

To obtain the value of $\rho_w(\lambda)$ in (1), four quantities have to be estimated:

1) Rayleigh reflectance $\rho_r(\lambda)$,
2) Reflectance of $\rho_a(\lambda) + \rho_{ra}(\lambda)$,
3) Value of $t(\lambda)$, and
4) Whitecap reflectance $\rho_{wc}(\lambda)$.

In the following four sections, some updates are discussed for the aerosol lookup tables $\rho_a(\lambda) + \rho_{ra}(\lambda)$, the atmospheric diffuse transmittance tables $t(\lambda)$, modifications in computing $\epsilon(\lambda_i, \lambda_j)$ when its value lies outside of the model range, and modifications in computing the whitecap reflectance contribution $\rho_{wc}(\lambda)$.

8.3 AEROSOL LOOKUP TABLES

Before the reprocessing (prior to August 1998), the SeaWiFS aerosol lookup tables were generated using 12 aerosol models with 8 aerosol optical thicknesses (0.05, 0.1, 0.15, 0.2, 0.3, 0.4, 0.6, and 0.8) and various solar and viewing geometries. The 12 aerosol models are Maritime, Coastal, and Tropospheric with the relative humidity (RH) of 50%, 70%, 90%, and 99%. The Maritime and Tropospheric aerosol models are from Shettle and Fenn (1979), whereas the Coastal model is derived from their works and is described in Gordon and Wang (1994b). These aerosol models are believed to be representative of the aerosol optical properties over the ocean. Table 1 provides the 12 aerosol model name, model number, and its corresponding symbol used before the reprocessing. These 12 aerosol models were used as candidates for generating the aerosol lookup tables for the atmospheric corrections. Figures 1a and 1b provide examples of $\epsilon(\lambda, 865)$ as a function of wavelength, λ, for these 12 aerosol models. Figure 1a is for the case of the solar zenith angle $\theta_0 = 0°$ and a viewing angle of $\theta_0 = 45°$, whereas Fig. 1(b) is for $\theta_0 = 60°$ with a viewing angle of $\theta_0 = 45°$ and a relative azimuthal angle of $\phi = 90°$. As discussed in the previous section, the $\epsilon(\lambda, 865)$ values as shown in Figs. 1a and 1b were used as a guide to select the aerosol model, and its optical and radiative properties were extrapolated from the SeaWiFS NIR bands into the visible spectrum in the atmospheric corrections. As shown in Figs. 1a and 1b, the T50 and M99 aerosol models give the highest and the lowest $\epsilon(\lambda, 865)$ values within these 12 aerosol models, respectively. These two aerosol models, therefore, were taken as default models as such that, if the retrieved $\epsilon(765, 865)$ value is higher (lower) than the value predicted by the T50 (M99) model, the retrieval model is defaulted to the T50 (M99) aerosols. Figures 1a and 1b show that, in the single scattering case, for the M99 model the aerosol reflectance at 412 nm contributes a factor of approximately 0.85–0.93 at 865 nm, while for the T50 model, the aerosol reflectance at the 412 nm wavelength is a factor of approximately 2.2–2.4 higher than at the 865 nm wavelength.

In the SeaWiFS data processing, however, there was evidence that some new aerosol models need to be included, in particular, for the optical properties with lower $\epsilon(\lambda, 865)$ values.

1. It was found that there was a significant number of pixels defaulting to select the M99 aerosol models, indicating that the lowest $\epsilon(765, 865)$ value predicted by the M99 model is still too high. For example, some case studies showed that about 35–40% retrievals defaulted to the M99 aerosol model.
2. It appeared that SeaWiFS retrieved more pixels associated with the negative water-leaving reflectance at the short wavelengths than at the long wavelengths, which indicated that probably for some cases, the aerosol contributions at the short wavelengths were overestimated.

It is apparently necessary to update the aerosol lookup tables. Following Gordon (pers. comm.), the Oceanic aerosol model from Shettle and Fenn (1979) was added into the candidate models. During the second reprocessing (August 1998–December 1999), the C70 and T70 models were replaced by the Oceanic aerosols with the relative humidity at 90% and 99% (O90 and O99, respectively). It was found, however, that in some cases (depending on the solar

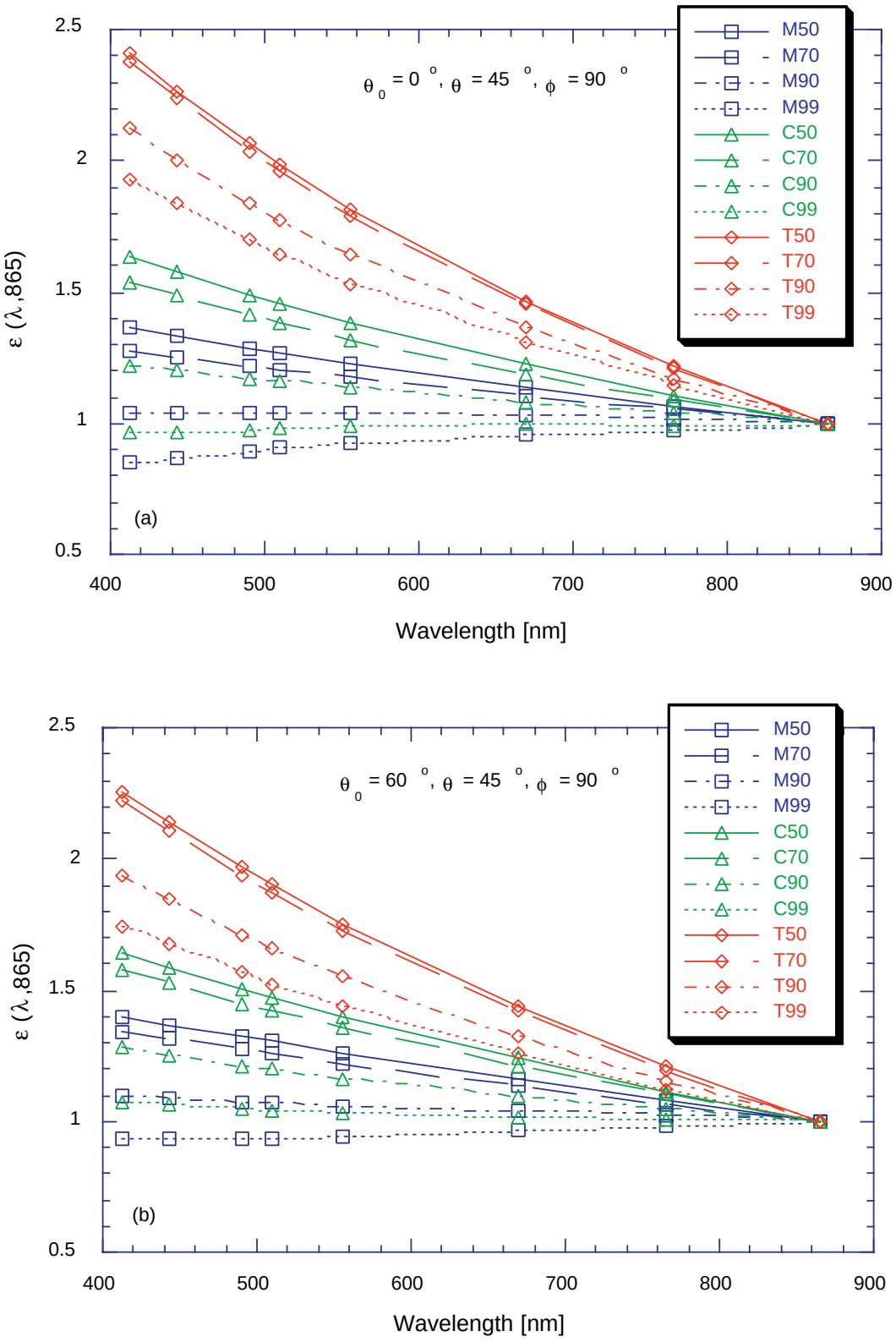

Fig. 1. The $\epsilon(\lambda, 865)$ value as a function of wavelength λ, for the 12 aerosol models used before the reprocessing for the sensor zenith angle of $\theta = 45°$, and the solar zenith angle of **a)** $\theta_0 = 0°$ and **b)** $\theta_0 = 60°$.

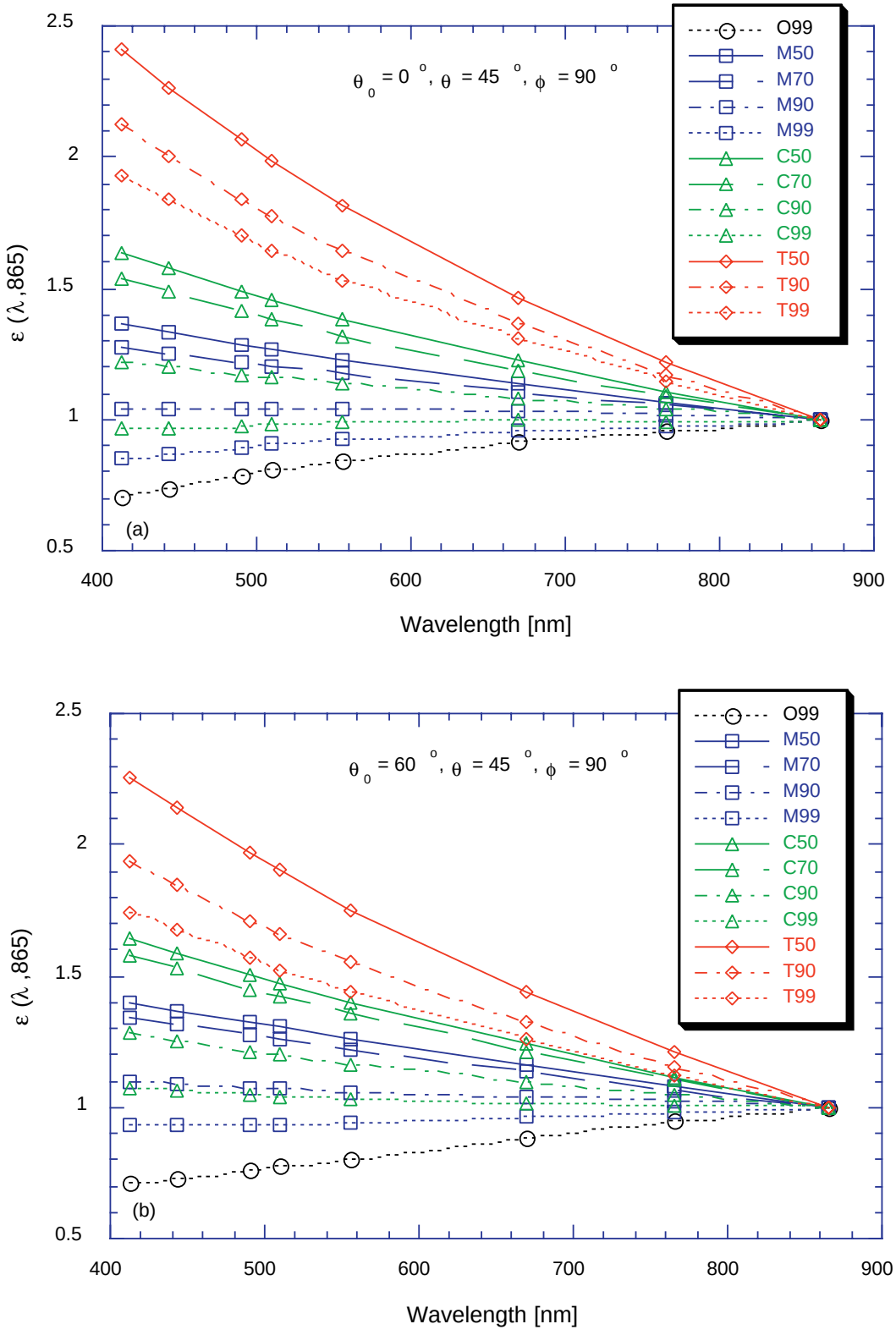

Fig. 2. The $\epsilon(\lambda, 865)$ value as a function of wavelength λ, for the 12 aerosol models used in the updated aerosol lookup tables for the sensor zenith angle of $\theta = 45°$, and the solar zenith angle of **a)** $\theta_0 = 0°$ and **b)** $\theta_0 = 60°$.

Table 1. The 12 aerosol models used before the reprocessing.

Model Number	*Aerosol Model*	*Relative Humidity* [%]	*Symbol*
1–4	Maritime	50, 70, 90, and 99	M50 to M99
5–8	Coastal	50, 70, 90, and 99	C50 to C99
9–12	Tropospheric	50, 70, 90, and 99	T50 to T99

and viewing geometry), the ϵ values predicted by the O90 model intersect with that of the M99 model as a function of the wavelength, e.g., the O90 model predicts a higher ϵ value at 765 nm and a lower value at 443 nm than those of the M99 model. This leads to discontinuities in the SeaWiFS derived products. In the third reprocessing, therefore, only the T70 model was replaced by the O99 model. The number of aerosol models is still kept as 12. Table 2 shows the 12 aerosol models used in the updated aerosol lookup tables. Using the same solar and viewing geometries as in Fig. 1, Figs. 2a and b provide the values of $\epsilon(\lambda, 865)$ as a function of wavelength λ for the updated aerosol models.

With the Oceanic aerosol model, the lowest $\epsilon(\lambda, 865)$ value is expanded. The O99 model predicts a factor of approximately 0.7 single scattering aerosol reflectance contribution at 412 nm as at 865 nm; this value is lower than the value from the M99 model (≈0.85–0.93). Inclusion of the new models decreased the number of pixels being processed with the default aerosol model by more than one half.

In addition, the computation of the $\epsilon(\lambda, 865)$ values has been modified for cases where the retrieved $\epsilon(765, 865)$ value is lower than the lowest values of the 12 models predicted (O99 model). Instead of using the default model to compute $\epsilon(\lambda, 865)$, an analytical formula (Wang and Gordon 1994) was used with retrieved $\epsilon(765, 865)$ values to estimate $\epsilon(\lambda, 865)$, i.e.,

$$\epsilon(\lambda, 865) \;=\; \exp\left(\log_e\left[\epsilon(765, 865)\right]\frac{865-\lambda}{100}\right). \qquad (4)$$

With these changes, the retrieval results are significantly improved by using the updated aerosol lookup tables (Robinson et al. 2000 ??? Vol. 10 ???).

8.4 TRANSMITTANCE TABLES

Because the atmospheric diffuse transmittance values [$t(\lambda)$ in (1)] depend on the aerosol models, it is, therefore, necessary to update the transmittance tables with the updated aerosol models, i.e., including the transmittance tables for both the O99 model. Also, in the old tables (prior to August 1998), there was an error in the atmospheric diffuse transmittance tables, in which the Fresnel-reflecting ocean surface was mistakenly not included in the computations. This caused the SeaWiFS retrieved normalized water-leaving radiance to depend strongly on the SeaWiFS scan angle, in particular, at the SeaWiFS scan edges. This error was corrected in the updated diffuse transmittance tables. The reprocessing results show that the normalized water-leaving radiance now has no obvious dependence on the SeaWiFS scanning angles (R.E. Eplee, pers. comm.).

8.5 WHITECAP CONTRIBUTIONS

As discussed in Sect. 8.2, the whitecap contribution $\rho_{wc}(\lambda)$ in the SeaWiFS imagery is estimated by using a reflectance model (Koepke 1984) with the input of sea-surface wind speed (Gordon and Wang 1994a). It is assumed that the whitecap is white, i.e., the foam reflectance is independent of the wavelength. The *in situ* measurements, however, show a significant uncertainty in $\rho_{wc}(\lambda)$ with the sea-surface wind speed (e.g., Monahan 1971). The measurement data are particularly noisy for the sea-surface wind speed greater than 7–8 $\mathrm{m\,s^{-1}}$, in which the uncertainty is usually greater than 100% (Fig. 1 in Gordon and Wang 1994a).

In recent studies, both Frouin et al. (1996) and Moore et al. (1998) found that contrary to the previous measurements, the whitecap reflectance is spectrally dependent. The reflectance contributions are significantly smaller at the near-infrared than in the visible, because of the stronger ocean water absorption at the longer wavelengths. This reduces the reflected photons from the submerged bubbles. The SeaWiFS observations also show that the whitecap reflectance model, used in the atmospheric corrections, likely overestimated the whitecap contributions significantly, in particular, for the larger sea-surface wind speed. The overcorrection was particularly evident in very clear open ocean scenes with high surface wind, which resulted in low normalized water-leaving radiance retrievals.

The SeaWiFS Project has adopted the Frouin et al. (1996) results (with updates) for the spectral dependence, and the results from Moore et al. 2000) for the magnitude of the whitecap contributions. This leads to the reduction of the whitecap radiance contributions for the SeaWiFS bands 1–8 by factors of 0.4, 0.4, 0.4, 0.4, 0.4, 0.3557, 0.3040, and 0.2580, respectively, relative to the values estimated using Gordon and Wang (1994a). The whitecap radiance for wind speeds greater than 8 $\mathrm{m\,s^{-1}}$ are set equal to the value computed at 8 $\mathrm{m\,s^{-1}}$. Results from *in situ* measurements showed similar characteristics (Moore et al. 2000). It is believed, however, that some validation efforts with more experimental data are needed to further

Table 2. The updated 12 aerosol models used in the reprocessing.

Model Number	*Aerosol Model*	*Relative Humidity* [%]	*Symbol*
1	Oceanic	99	O99
2-5	Maritime	50, 70, 90, and 99	M50 to M99
6-9	Coastal	50, 70, 90, and 99	C50 to C99
10-12	Tropospheric	50, 90, and 99	T50, T90, and T99

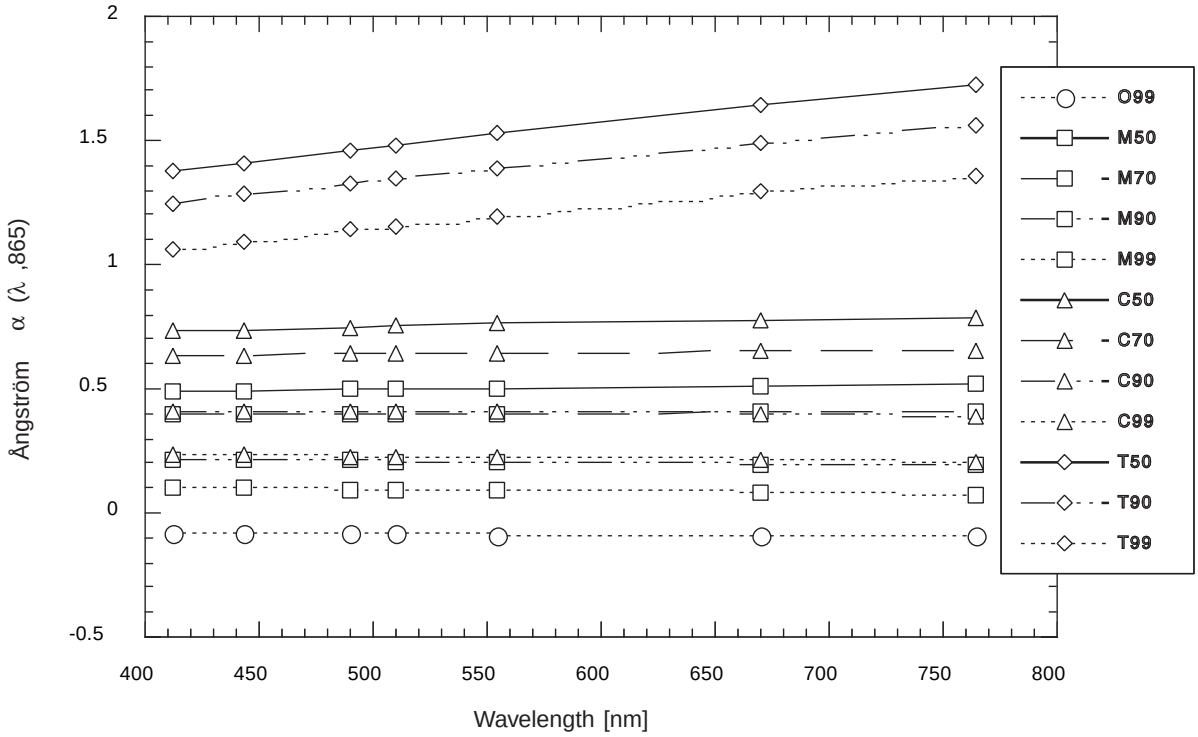

Fig. 3. The $\epsilon(\lambda, 865)$ value as a function of wavelength λ, for the SeaWiFS updated 12 aerosol models.

fine tune the foam reflectance model. Also, evaluations of the National Center for Environmental Prediction (NCEP) wind speeds using buoy winds near Hawaii and Bermuda show very good agreement, and differences between SeaWiFS and the Bermuda Test Bed Mooring (BTBM) water-leaving radiances were uncorrelated to wind speed (S. Bailey, pers. comm.) which suggests that the $8\,\mathrm{m\,s^{-1}}$ limit is not introducing a bias in the SeaWiFS products. In fact, it is better to underestimate foam radiance than to overestimate it (Gordon and Wang 1994a). The residual will be included in the aerosol radiance.

8.6 NEW RAYLEIGH TABLES

New Rayleigh radiance lookup tables for SeaWiFS' eight spectral bands were generated using the method developed by Gordon and Wang (1992) for the various ocean surface wind speeds. A bidirectionally shadowing factor for a collection of individual wind-ruffled facets (Gordon and Wang 1992) was used in all computations. This new wind-speed dependent Rayleigh tables have been implemented in the. Prior to the third reprocessing, Rayleigh tables were generated with a flat ocean surface assumption (where the wind speed is 0). The Rayleigh radiance tables were generated at eight ocean surface wind speeds corresponding to 0, 1.9, 4.2, 7.5, 11.7, 16.9, 22.9, and 30.0 $\mathrm{m\,s^{-1}}$, respectively. Tests showed that, with the new Rayleigh tables, the SeaWiFS-derived ocean color products are significantly improved, in particular, for cases of the larger solar zenith angles, i.e., θ_0 >60°. A detailed study for the effects of the surface roughness on the SeaWiFS derived ocean color products is currently underway.

8.7 ÅNGSTRÖM EXPONENT

The aerosol Ångström exponent is widely used in the atmospheric aerosol and radiation community. For two

wavelengths at λ_i and λ_j, the Ångström exponent is defined as

$$\frac{\tau_a(\lambda_i)}{\tau_a(\lambda_j)} = \left(\frac{\lambda_j}{\lambda_i}\right)^{\alpha(\lambda_i,\lambda_j)}, \quad (5)$$

or

$$\alpha(\lambda_i,\lambda_j) = \frac{\log_e\left(\frac{\tau_a(\lambda_i)}{\tau_a(\lambda_j)}\right)}{\log_e\left(\frac{\lambda_j}{\lambda_i}\right)}, \quad (6)$$

where $\tau_a(\lambda_i)$ and $\tau_a(\lambda_j)$ are aerosol optical thicknesses measured at λ_i and λ_j, respectively. The Ångström exponent, which is independent of the solar and viewing geometry, can be used to relate the aerosol microphysical properties (particle size) and its optical spectral dependence. Figure 3 provides values of $\alpha(\lambda, 865)$ as a function of wavelength, λ, for the 12 SeaWiFS updated aerosol models. Apparently, the $\alpha(\lambda, 865)$ value is nearly independent of the wavelength, in particular for the Oceanic, Maritime, and Coastal aerosol models.

With the retrieved two aerosol models in the atmospheric correction process, the SeaWiFS $\alpha(\lambda_i, 865)$ can be easily derived, that is,

$$\alpha(\lambda_i, 865) = (1-r)\alpha^a(\lambda_i, 865) + r\alpha^b(\lambda_i, 865), \quad (7)$$

where $\alpha^a(\lambda_i, 865)$ and $\alpha^b(\lambda_i, 865)$ are, respectively, the Ångström exponent from derived models a and b, and the r is the ratio between two aerosol models from the retrieved ϵ values. The SeaWiFS $\alpha(\lambda_i, 865)$ retrieval routine can be very easily implemented in the SeaWiFS data processing.

It was decided that the $\alpha(510, 865)$ data will be routinely retrieved and archived. The reasons to choose the wavelength at 510 nm are that it is closely matched with the ground *in situ* measurement data (e.g., AERONET data) and it gives a good approximation to be used in deriving aerosol optical thickness at other SeaWiFS wavelengths (e.g., 412 nm). Nevertheless, one can easily modify the SeaWiFS Data Analysis System (SeaDAS) code and obtain $\alpha(\lambda_i, 865)$ in any of the SeaWiFS wavelengths.

REFERENCES

Frouin, R., M. Schwindling, and P.Y. Deschamps, 1996: Spectral reflectance of sea foam in the visible and near infrared: *In situ* measurements and remote sensing implications. *J. Geophys. Res.,* **101,** 14,361–14,371.

Gordon, H.R., and M. Wang, 1992: Surface roughness considerations for atmospheric correction of ocean color sensors. 1: Rayleigh scattering component. *Appl. Opt.,* **31,** 4,247–4,260.

Gordon, H.R., and M. Wang, 1994a: Influence of oceanic whitecaps on atmospheric correction of ocean-color sensors. *Appl. Opt.,* **33,** 7,754–7,763.

Gordon, H.R., and M. Wang, 1994b: Retrieval of water-leaving radiance and aerosol optical thickness over the oceans with SeaWiFS: A preliminary algorithm. *Appl. Opt.,* **33,** 443–452.

Hooker, S.B., W.E. Esaias, G.C. Feldman, W.W. Gregg, and C.R. McClain, 1992: An Overview of SeaWiFS and Ocean Color. *NASA Tech. Memo. 104566, Vol. 1,* S.B. Hooker and E.R. Firestone, Eds., NASA Goddard Space Flight Center, Greenbelt, Maryland, 24 pp.

Koepke, P., 1984: Effective reflectance of oceanic whitecaps. *Appl. Opt.,* **23,** 1,816–1,824.

McClain, C.R., M.L. Cleave, G.C. Feldman, W.W. Gregg, S.B. Hooker, and N. Kuring, 1998: Science quality SeaWiFS data for global biosphere research. *Sea Technol.,* 10–16.

Monahan, E.C., 1971: Oceanic whitecaps. *J. Phys. Oceanogr.,* **1,** 139–144.

Moore, K.D., K.J. Voss, and H.R. Gordon, 1998: Spectral reflectance of whitecaps: Instrumentation, calibration, and performance in coastal waters. *J. Atmos. Ocean. Tech.,* **15,** 496–509.

Moore, K.D., K.J. Voss, and H.R. Gordon, 2000: Spectral reflectance of whitecaps: Their contribution to water-leaving radiance. *J. Geophys. Res.,* **105,** 6,493–6,499.

Robinson, W.D., C.R. McClain, G.M. Schmidt, and H. Qi, 2000: "Changes made in the operational SeaWiFS processing." ??? Vol. 10 ???

Shettle, E.P., and R.W. Fenn, 1979: Models for the Aerosols of the Lower Atmosphere and the Effects of Humidity Variations on Their Optical Properties. *AFGL-TR-79-0214,* U.S. Air Force Geophysics Laboratory, Hanscom Air Force Base, Massachusetts, 94 pp.

Wang, M., 1999: Atmospheric correction of ocean color sensors: Computing atmospheric diffuse transmittance. *Appl. Opt.,* **38,** 451–455.

Wang, M., and H.R. Gordon, 1994: A simple, moderately accurate, atmospheric correction algorithm for SeaWiFS. *Remote Sens. Environ.,* **50,** 231–239.

Yang, H., and H.R. Gordon, 1997: Remote sensing of ocean color: assessment of water-leaving radiance bidirectional effects on atmospheric diffuse transmittance. *Appl. Opt.,* **36,** 7,887–7,897.